Next-Generation Snow Cover Monitoring in Near Real Time: Evaluating the EUMETSAT H SAF H43 Product from MTG-FCI across the European Alps

Semih Kuter [1], Çağrı Hasan Karaman [2], Mustafa Berkay Akpınar [2], Zuhal Akyürek [3,4]

[1] Çankırı Karatekin University, Faculty of Forestry, Dept. of Forest Engineering, Türkiye - semihkuter@karatekin.edu.tr
[2] HidroSAF Ltd., Middle East Technical University (METU) Technopolis, Türkiye - cagrikaraman@hidrosaf.com, berkay.akpinar@hidrosaf.com
[3] METU, Faculty of Engineering, Dept. of Civil Engineering, Türkiye - zakyurek@metu.edu.tr
[4] METU, Graduate School of Natural and Applied Sciences, Dept. of Geodetic and Geographic Information Technologies, Türkiye

Keywords: Remote Sensing of Snow, EUMETSAT, H SAF, Meteosat Third Generation, Flexible Combined Imager.

Abstract

Reliable snow cover mapping in mountainous regions is critical for hydrology, climate monitoring, and hazard risk management. This study presents the initial evaluation of the EUMETSAT H SAF H43 snow cover extent product—the first derived from the Flexible Combined Imager (FCI) aboard Meteosat Third Generation (MTG)—over the European Alps. The assessment was performed by comparing H43 with its predecessor H34, using daily MODIS MOD10A1 NDSI-based binary snow maps as the reference for the 2024–2025 winter season. Evaluation metrics, including Probability of Detection (POD), False Alarm Ratio (FAR), and Overall Accuracy (ACC), were calculated based on pixel-level agreement across December to February. To investigate terrain-dependent classification performance, the spatial distribution of false alarms (B) and missed detections (C) was analyzed across elevation zones and terrain aspect classes derived from the MODIS 1 km MODDEM product. Wind rose visualizations revealed that both products exhibit classification uncertainty in mid-elevation ranges (1000–2000 m), with H34 showing higher miss rates and H43 slightly more false alarms. In higher elevation bands (≥2000 m), H43 demonstrated improved stability across slope orientations and generally lower error rates. These findings highlight the enhanced snow retrieval capability of the H43 product in complex alpine environments and support its application in near-real-time snow monitoring.

1. Introduction

Monitoring and mapping snow cover is essential for understanding the Earth's surface energy balance and the role of snow within the climate system (Akyurek *et al.*, 2023). Due to its high albedo, snow reflects a large fraction of incoming solar radiation back into the atmosphere (Kuter *et al.*, 2018; Tekeli *et al.*, 2005). This property plays a key role in regulating surface heating and cooling processes.

Among all land surface types, snow cover has the most pronounced effect on the surface energy balance (Chen *et al.*, 2021). Variations in snow cover—both in extent and duration—can significantly influence surface energy fluxes, thereby affecting climate patterns and related feedback mechanisms. Accurate and consistent snow cover mapping is therefore crucial for improving our understanding of these interactions and their implications for the global climate system (Takala *et al.*, 2011).

Near-real-time snow cover mapping is a critical capability for a range of applications, including hydrological forecasting, natural hazard management, and climate monitoring (Appel and Bach, 2003). Timely information on snow extent supports flood prediction during snowmelt periods, improves water resource planning, and aids in managing transportation and infrastructure risks in snow-affected regions (Parajka and Blöschl, 2008).

Satellite-based systems that deliver snow cover products within hours of observation allow decision-makers to respond more effectively to changing surface conditions. With advancements in satellite sensor technology and data processing chains, products such as those derived from the Meteosat Third Generation Flexible Combined Imager (MTG-FCI) (Guggenmoser *et al.*, 2024) now offer improved spatial and temporal resolution, enabling consistent daily monitoring over large geographic areas. These capabilities enhance the operational use of satellite snow products in both regional and global monitoring systems.

This study is conducted within the framework of the EUMETSAT Satellite Application Facility on Support to Operational Hydrology and Water Management (H SAF), which focuses on the development of operational satellite-derived products for hydrological and environmental applications. In this context, we aim to assess the performance of the newly introduced H SAF H43 snow cover extent (SCE) product generated from MTG-FCI over the European Alps. The performance of H43 is also compared to that of H34, the previous SCE product derived from MSG-SEVIRI.

2. Materials and Methods

2.1 MTG-FCI and H43 Snow Cover Extent Product

The Flexible Combined Imager (FCI) onboard Meteosat Third Generation (MTG) offers major improvements over its predecessor, SEVIRI on Meteosat Second Generation (MSG) (Yannig *et al.*, 2015). FCI provides 16 spectral bands with higher spatial resolution (1–2 km at nadir) and a faster refresh rate (every 10 minutes), compared to SEVIRI's 12 bands, 3 km resolution, and 15-minute updates (EUMETSAT, 2025). These enhancements improve the detection of snow, clouds, and land surface conditions, making MTG-FCI especially valuable for near-real-time snow monitoring over complex terrain, where the older MSG-SEVIRI-based products had known limitations (Holmlund *et al.*, 2021).

The H43 product represents a significant advancement in near-real-time snow monitoring, offering snow cover maps every 10 minutes at a spatial resolution of approximately 2 km at nadir. It is generated from observations acquired by FCI onboard the MTG satellite. The product combines two complementary

retrieval schemes to generate a seamless daily composite: i) the algorithm designed for flat and forested regions, developed by the Finnish Meteorological Institute, and ii) the algorithm tailored for mountainous areas, developed by the Turkish State Meteorological Service in collaboration with the Middle East Technical University (H-SAF_H43_PUM, 2025).

Once the required channel data from the MTG-FCI sensor are acquired, the H SAF H43 processing chain generates separate snow cover products for flat/forested and mountainous regions, which are then merged into a single composite. This end-to-end process is completed within approximately three hours, ensuring timely availability of the final daily product at 01:00 UTC (H-SAF_H43_ATBD, 2025).

Such processing efficiency supports the near-real-time nature of H43 and enhances its operational value for applications that require rapid snow cover updates, particularly in hydrology, risk management, and environmental monitoring.

Both approaches utilize the strong reflectance of snow in the 0.4–0.5 µm spectral range, along with visible and infrared indices, to distinguish snow from cloud and land under varying illumination conditions. Through this validation study, we aim to assess the accuracy, robustness, and potential of the H43 product for operational snow monitoring in complex alpine terrain.

On the other hand, the H SAF H34 product is the previous operational version SCE product, derived from the SEVIRI sensor onboard Meteosat Second Generation (MSG). It provides snow detection at ~3 km spatial resolution at nadir, with updates every 15 minutes. H34 uses a multispectral thresholding approach based on visible and infrared channels to classify snow, land, and cloud surfaces (H-SAF_H34_PUM, 2023).

As the direct predecessor of the H43 product, H34 served as the foundation for the development of snow retrieval methods within the H SAF framework. While it provided valuable near-real-time snow cover information for several years, its limitations—particularly in spatial resolution and cloud discrimination—have been addressed in the next-generation H43 product, which utilizes enhanced capabilities of the MTG-FCI sensor.

2.2 Spatial and Temporal Domain for the Validation

The validation of the H SAF H43 SCE product was conducted over the European Alps between 1 December 2024 and 28 February 2025. This region was selected due to its complex topography, frequent snow events, and variable land cover, providing a rigorous test environment for snow detection (cf. Figure 1).

The study area spans approximately 445,470 km², bounded by 43° 39' N to 48° 30' N latitude and 5° 6' E to 16° 17' E longitude. Based on the H43 mountain and water masks, the terrain consists of 37% mountainous, 51% flatland, and 12% water-covered areas. Elevation ranges from valley floors to peaks exceeding 4,500 meters, with an average elevation of 1,607 meters. These diverse conditions make the Alps a key region for assessing the accuracy and robustness of satellite-based snow products.

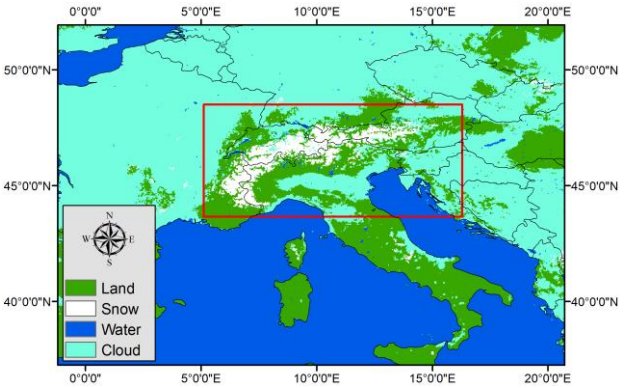

Figure 1. Spatial domain for the validation: H43 product over European Alps on 9 Jan 2025.

2.3 MODIS Reference Dataset

The validation of the H43 SCE product is carried out using reference snow cover maps derived from the MODIS MOD10A1 NDSI Collection 6.1 dataset (Riggs *et al.*, 2019). MOD10A1 is a daily global snow product from NASA's Terra satellite and has been extensively validated against both in-situ and satellite observations, with reported accuracies ranging from 77% to 100% (Gascoin *et al.*, 2015; Parajka and Blöschl, 2006). Despite some limitations due to cloud cover and snowpack variability (Brubaker *et al.*, 2005), its 500 m spatial resolution makes it a suitable reference for large-scale snow monitoring. MODIS data for the period 1 December 2024 to 28 February 2025 were downloaded from NASA's AppEEARS platform (hiips://appeears.earthdatacloud.nasa.gov/).

Normalized Difference Snow Index (NDSI) helps differentiate snow from other surfaces like clouds, water, and vegetation. For validation, the MOD10A1 NDSI data are resampled and aggregated to match the H43 resolution (i.e., ~2 km at nadir), following these steps, as also indicated in Kuter *et al.* (2025):

- Pixels with NDSI ≥ 0.4 are classified as snow; others are labelled as non-snow.
- Classifications are aggregated within each H43 pixel footprint.
- The dominant class (snow, non-snow, cloud, water, unclassified, or no data) is assigned to the H43 pixel.
- In the case of a tie between snow and other classes, the pixel is labelled as snow to avoid underestimation.
- The same methodology also applies for H34, but within a ~3 km resolution.

A binary error matrix (i.e., contingency table; cf. Table 1) is employed to compare the H43 (as well as H34) product with the MODIS-derived reference dataset.

The evaluation is based on key statistical metrics, including:

- Probability of Detection (POD): Measures the percentage of actual snow pixels correctly identified. Higher values indicate better detection (POD = A / (A + C)),
- False Alarm Ratio (FAR): Shows the proportion of falsely detected snow pixels. Lower values mean fewer errors (FAR = B / (A + B)), and
- Overall Accuracy (ACC): Represents the total percentage of correctly classified pixels, reflecting overall reliability (ACC = (A + D) / (A + B + C + D)) (Kuter *et al.*, 2025).

		Ground Truth (MODIS MOD10A1 NDSI)	
		Snow	**No Snow**
Satellite Product (H34/H43)	**Snow**	HITS (A)	FALSE ALARMS (B)
	No Snow	MISSES (C)	CORRECT NEGATIVES (D)

Table 1. Binary error matrix.

In addition, snow detection performance is analyzed with respect to land cover types using the MODIS MCD12Q1 dataset (Friedl *et al.*, 2010), in which similar land cover classes are grouped to improve clarity. This enables a more detailed assessment of how land surface characteristics affect classification accuracy.

3. Results and Discussions

Table 2 summarizes the minimum, maximum, and mean values of the statistical metrics for the European Alps, whereas Figure 2 presents the complete set of metrics together with the cloud cover fraction.

Metric	**H34**			**H43**		
	Min	**Max**	**Mean**	**Min**	**Max**	**Mean**
POD	0.2965	0.9556	0.7824	0.2272	0.9834	0.8466
FAR	0.0029	0.2006	0.0743	0.0064	0.2419	0.0695
ACC	0.7848	0.9758	0.9209	0.7728	0.9800	0.9343

Table 2. Comparative Statistical Metrics of H34 and H43 for the European Alps

The results show that H43 consistently performs better than H34, exhibiting higher Probability of Detection (POD) and Overall Accuracy (ACC), while generally maintaining a slightly lower False Alarm Ratio (FAR). The lowest POD values were recorded in early December, likely due to increased cloud cover (Kuter *et al.*, 2025). Although both products achieved high ACC values, H43 showed closer agreement with the MODIS MOD10A1 NDSI reference data.

On a monthly basis, POD values for H43 and H34 were similar in December (around 0.77), but in January, H43 improved markedly to 0.92, while H34 remained relatively unchanged. By February, H43 reached its peak POD value of 0.95, reflecting enhanced snow detection performance. FAR values were lowest in December, indicating fewer false positives early in the season, but showed a slight increase in January and February, likely due to seasonal snow dynamics and melting events (Kuter *et al.*, 2025). Throughout the period, ACC remained high for both products, with H43 achieving a maximum value of 0.97 in February.

Cloud contamination had a noticeable effect on detection accuracy, particularly during early December and mid-February. Nonetheless, H43 demonstrated greater robustness under cloudy conditions compared to H34.

To complement the overall performance assessment, a terrain-based analysis was performed to explore the spatial distribution of classification errors—specifically false alarms (B) and missed detections (C)—in relation to elevation and terrain aspect in the validation region (cf. Figure 3). This evaluation provides insights into the topographic sensitivities of the H34 and H43 snow products and highlights systematic retrieval challenges in mountainous environments. Terrain elevation and aspect information were derived from the 1 km resolution MODIS MODDEM digital elevation model (Wolfe, 2013).

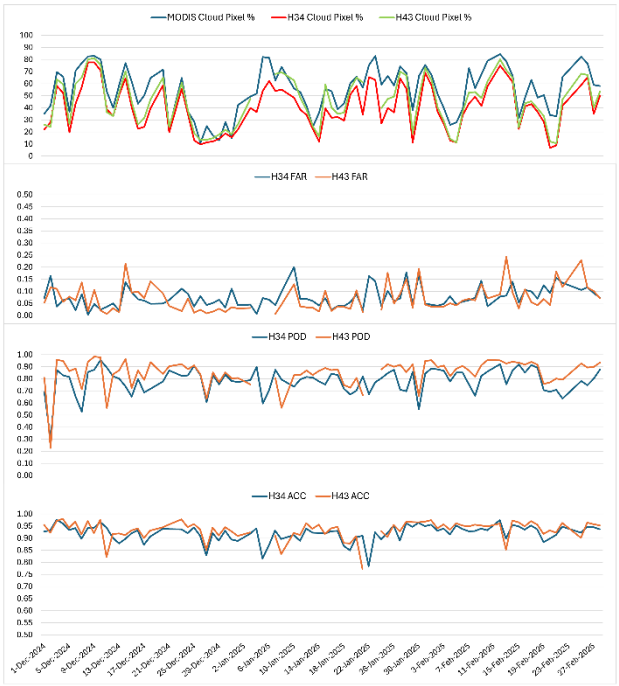

Figure 2. Time series of cloud cover percentage, FAR, POD, and ACC over the European Alps (1 December 2024–28 February 2025), shown from top to bottom.

Within the 1000–1500 m elevation band—where snow cover is often intermittent—H34 exhibited a slightly higher miss rate (~1.58%) than H43 (~1.46%), indicating more conservative snow detection. Conversely, H43 recorded more false alarms (~0.45%) than H34 (~0.34%), suggesting a tendency to overestimate snow presence under variable terrain or radiometric conditions. North- and east-facing slopes amplified these differences, with H34 prone to misses and H43 to false alarms, reflecting differing sensitivities to terrain shading and illumination.

At 1500–2000 m, both products showed moderate uncertainty, but H34 again had higher misses (~1.71% vs. 1.24%), while H43 showed more false alarms (~0.37% vs. 0.21%). North- and east-facing aspects remained dominant contributors to errors in both products.

In the 2000–2500 m range, H34 missed more snow (~1.16%) than H43 (~0.60%), possibly due to cloud contamination or spectral confusion with high-reflectance surfaces. False alarms were notably higher in H34 (~0.74%) than in H43 (~0.12%). H34's errors were concentrated on shaded or variably illuminated slopes, while H43 maintained stable performance across aspects.

In the highest elevation class (≥2500 m), H34 continued to miss more snow (~1.16%) than H43 (~0.60%), while false alarms remained low for both (H43: ~0.08%, H34: ~0.03%). H34's aspect-related errors were most pronounced on north-, northeast-, and southeast-facing slopes, suggesting reduced sensitivity to snow in shaded or dynamically melting terrain. H43 exhibited consistent accuracy across all aspects, indicating more robust performance in high-altitude conditions.

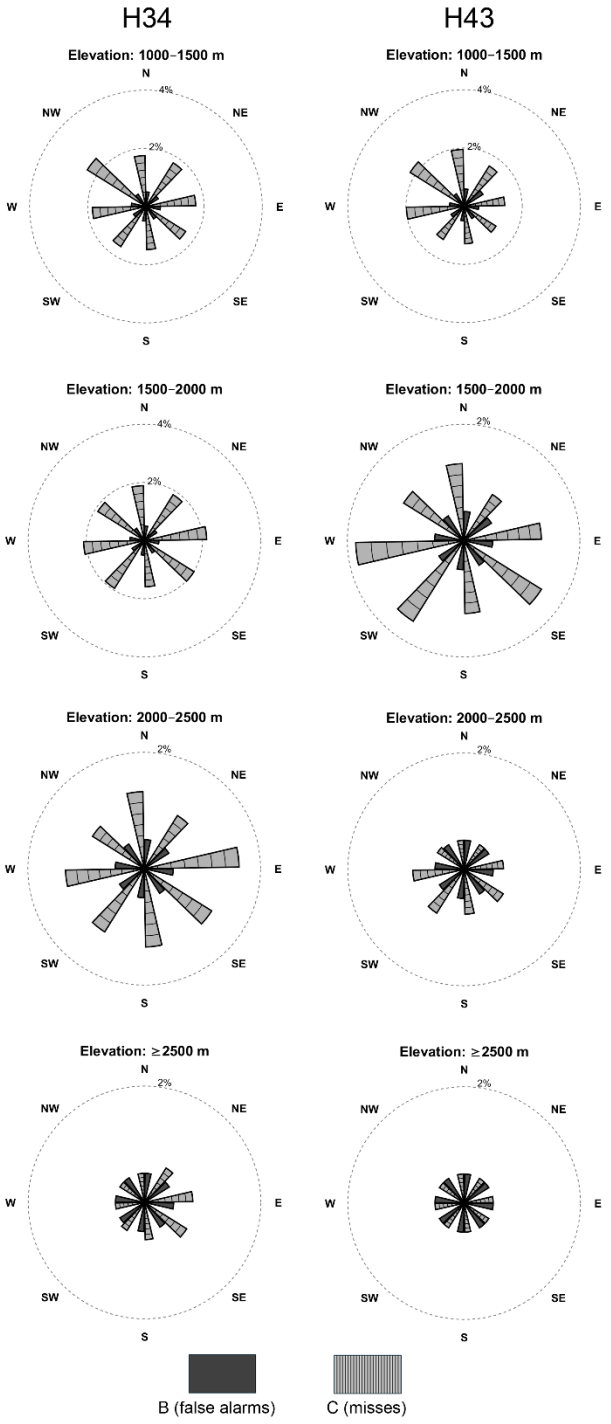

Figure 3. Wind rose diagrams of false alarms (B) and misses (C) with respect to elevation and aspect.

Land cover type plays a critical role in the accuracy of snow cover retrieval from optical satellite observations. In forested areas, the presence of dense canopy can obscure the underlying snow, leading to underestimation of snow extent due to limited surface visibility in the visible and near-infrared spectral bands (Klein *et al.*, 1998). Mixed pixels containing both vegetation and snow further complicate the spectral signature, reducing the contrast between snow-covered and snow-free surfaces. Conversely, open land cover types such as grasslands, barren ground, and agricultural fields typically allow unobstructed detection of snow, resulting in higher retrieval accuracy (Hall *et al.*, 1998). These effects are especially pronounced in moderate-resolution sensors, where sub-pixel heterogeneity influences the classification outcome.

The influence of land cover variability on snow detection was clearly observed in the Alps in Figure 4, especially in areas dominated by forests and mixed vegetation, where snow classification tends to be more challenging. Land cover classes such as Evergreen and Mixed Forests showed lower POD values for both H34 and H43, primarily due to snow being obscured by dense tree canopies. In contrast, open landscapes like grasslands and shrublands yielded higher POD values, reflecting more accurate snow detection where vegetation interference is minimal. Compared to H34, the H43 product demonstrated a reduction in false alarms across forested areas, contributing to improved overall classification accuracy.

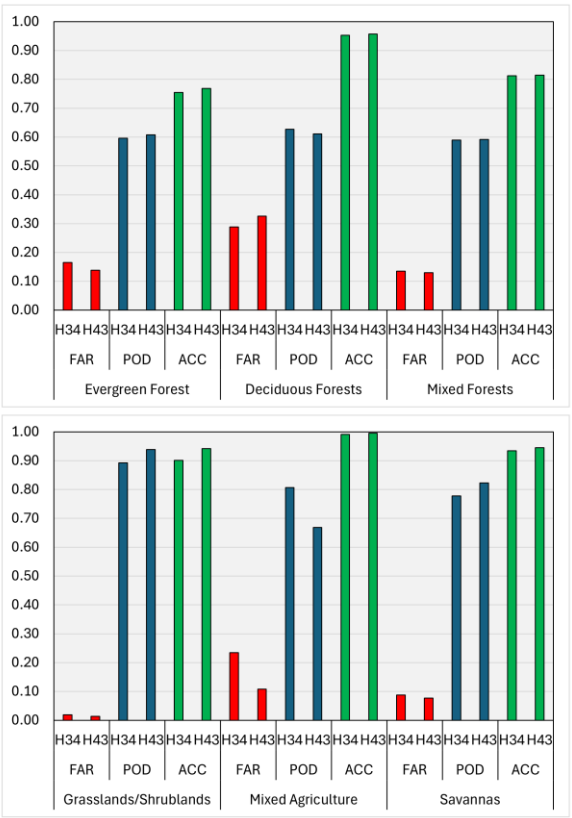

Figure 4. FAR, POD, and ACC metrics across different land cover types in the European Alps.

4. Conclusions

The validation results show that H43 outperforms H34 in terms of snow detection performance and classification reliability. Over the European Alps, H43 consistently achieves higher POD and ACC, with particularly strong results over open land cover types such as grasslands, shrublands, and bare areas. Moreover, H43 generally maintains a low FAR, with noticeable improvements in forested and mixed vegetation classes, where optical snow detection is often challenged by canopy effects and mixed pixels.

The land cover-based analysis confirms that surface type significantly influences snow retrieval accuracy. In forested landscapes, snow is frequently obscured by vegetation, leading to increased uncertainty, while open terrain allows clearer spectral separation between snow and background surfaces.

Across the diverse land cover types of the Alps, H43 showed greater stability and better agreement with reference data than H34. Moreover, it demonstrated enhanced resilience to cloud contamination, which is common in mountainous environments and often reduces retrieval performance.

Although this study is limited to a three-month winter period (December 2024 to February 2025) and a single geographic region, the results highlight the improved accuracy and consistency of H43 in complex alpine terrain. These findings support its operational use for snow monitoring in mountainous areas. Future validation studies extending into the accumulation and melt periods will be essential to assess the seasonal robustness of H43 and identify any region-specific limitations under varying surface conditions.

References

Akyurek, Z., Kuter, S., Karaman, Ç. H. and Akpınar, B. (2023). Understanding the Snow Cover Climatology over Turkey from ERA5-Land Reanalysis Data and MODIS Snow Cover Frequency Product. *Geosciences, 13*(10).

Appel, F. and Bach, H. (2003, 21-25 July 2003). *Near-real-time derivation of snow cover maps for hydrological modeling using operational remote sensing data.* Paper presented at the IGARSS 2003. 2003 IEEE International Geoscience and Remote Sensing Symposium. Proceedings (IEEE Cat. No.03CH37477).

Brubaker, K. L., Pinker, R. T. and Deviatova, E. (2005). Evaluation and Comparison of MODIS and IMS Snow-Cover Estimates for the Continental United States Using Station Data. *Journal of Hydrometeorology,* 6(6), pp. 1002–1017.

Chen, X., Yang, Y. and Yin, C. (2021). Contribution of Changes in Snow Cover Extent to Shortwave Radiation Perturbations at the Top of the Atmosphere over the Northern Hemisphere during 2000–2019. *Remote Sensing Letters,* 13(23), pp. 4938.

EUMETSAT. (2025). MTG FCI Level 1C Data Guide. Retrieved on 19 May, 2025, from hiips://user.eumetsat.int/resources/user-guides/mtg-fci-level-1c-data-guide.

Friedl, M. A., Sulla-Menashe, D., Tan, B., Schneider, A., Ramankutty, N., Sibley, A. and Huang, X. (2010). MODIS Collection 5 global land cover: Algorithm refinements and characterization of new datasets. *Remote Sensing of Environment,* 114(1), pp. 168-182.

Gascoin, S., Hagolle, O., Huc, M., Jarlan, L., Dejoux, J. F., Szczypta, C., Marti, R. and Sánchez, R. (2015). A snow cover climatology for the Pyrenees from MODIS snow products. *Hydrol. Earth Syst. Sci.,* 19(5), pp. 2337-2351.

Guggenmoser, T., Lamarre, D., Aminou, D., Braembussche, P. V. D., Palacios, A., Champion, J., Bennett, I., Toledo, A. A., Ascani, L., Jorba, P., Finella, E., Fusco, G., Lattner, K., Feckl, R., Levin, T., Riegger, L., Miras, D., Abdon, S. and Sivelle, N. (2024, 7-12 July 2024). *Meteosat Third Generation Sounder (MTG-S) – Status of Spacecraft and Payload Development.* Paper presented at the IGARSS 2024 - 2024 IEEE International Geoscience and Remote Sensing Symposium.

H-SAF_H34_PUM. (2023). Product User Manual (PUM) for product H34 – SN-OBS-1G Snow detection (snow mask) by VIS/IR radiometry. *EUMETSAT Satellite Application Facility on Support to Operational Hydrology and Water Management.* Retrieved on 13 February, 2025, from hiips://hsaf.meteoam.it/Products/Detail?prod=H34.

H-SAF_H43_ATBD. (2025). Algorithm Theoretical Basis Document (ATBD) for product H43 – SE-D-FCI Snow detection (snow mask) MTG/FCI by VIS/IR radiometry. *EUMETSAT Satellite Application Facility on Support to Operational Hydrology and Water Management.* Retrieved on 13 February 2025, from hiips://hsaf.meteoam.it/CaseStudy/GetDocumentUserDocument?fileName=SAF_HSAF_ATBD-43_1_4.pdf&tipo=ATBD.

H-SAF_H43_PUM. (2025). Product User Manual (PUM) for product H43 – SE-D-FCI Snow detection (snow mask) MTG/FCI by VIS/IR radiometry. *EUMETSAT Satellite Application Facility on Support to Operational Hydrology and Water Management.* Retrieved on 30 August 2025, from hiips://hsaf.meteoam.it/CaseStudy/GetDocumentUserDocument?fileName=SAF_HSAF_PUM-43_1_5.pdf&tipo=PUM.

Hall, D., Foster, J., Verbyla, D., Klein, A. and Benson, C. (1998). Assessment of snow-cover mapping accuracy in a variety of vegetation-cover densities in central Alaska. *Remote Sensing of Environment,* 66(2), pp. 129-137.

Holmlund, K., Grandell, J., Schmetz, J., Stuhlmann, R., Bojkov, B., Munro, R., Lekouara, M., Coppens, D., Viticchie, B., August, T., Theodore, B., Watts, P., Dobber, M., Fowler, G., Bojinski, S., Schmid, A., Salonen, K., Tjemkes, S., Aminou, D. and Blythe, P. (2021). Meteosat Third Generation (MTG): Continuation and Innovation of Observations from Geostationary Orbit. *Bulletin of the American Meteorological Society,* 102(5), pp. E990-E1015.

Klein, A. G., Hall, D. K. and Riggs, G. A. (1998). Improving snow cover mapping in forests through the use of a canopy reflectance model. *Hydrological Processes,* 12(10), pp. 1723-1744.

Kuter, S., Akyürek, Z., Karaman, Ç. and Akpınar, B. (2025). Product Validation Report (PVR) for product SE-D-FCI (H43) Snow detection (snow mask) by VIS/NIR of MTG FCI. *EUMETSAT Satellite Application Facility on Support to Operational Hydrology and Water Management.* Retrieved on 30 August 2025, from hiips://hsaf.meteoam.it/CaseStudy/GetDocumentUserDocument?fileName=saf_hsaf_pvr-43_v1.1.pdf&tipo=PVR.

Kuter, S., Akyurek, Z. and Weber, G. W. (2018). Retrieval of fractional snow covered area from MODIS data by multivariate adaptive regression splines. *Remote Sensing of Environment,* 205, pp. 236-252.

Parajka, J. and Blöschl, G. (2006). Validation of MODIS snow cover images over Austria. *Hydrol. Earth Syst. Sci.,* 10(5), pp. 679-689.

Parajka, J. and Blöschl, G. (2008). Spatio-temporal combination of MODIS images – potential for snow cover mapping. *Water Resources Research,* 44(3).

Riggs, G. A., Hall, D. K. and Román, M. O. (2019). MODIS Snow Products Collection 6.1 User Guide Version 1.0. Retrieved on February 13, 2025, from hiips://modis-snow-ice.gsfc.nasa.gov/uploads/snow_user_guide_C6.1_final_revised_april.pdf.

Takala, M., Luojus, K., Pulliainen, J., Derksen, C., Lemmetyinen, J., Kärnä, J.-P., Koskinen, J. and Bojkov, B. (2011). Estimating northern hemisphere snow water equivalent for climate research through assimilation of space-borne radiometer data and ground-based measurements. *Remote Sensing of Environment,* 115(12), pp. 3517-3529.

Tekeli, A. E., Akyürek, Z., Şorman, A. A., Şensoy, A. and Şorman, Ü. (2005). Using MODIS snow cover maps in modeling snowmelt runoff process in the eastern part of Turkey. *Remote Sensing of Environment,* 97, pp. 216-230.

Wolfe, R. (2013). MODIS Land Digital Elevation Model and Land/Water Mask in the Sinusoidal Grid Version 6.0. *MODIS Science Team Support NASA Goddard Space Flight Center.* Retrieved on 13 Feb 2025, 2025, from hiips://landweb.modaps.eosdis.nasa.gov/data/userguide/DEM.pdf.

Yannig, D., Pascal, H., Mark, W., Mounir, L., Semen, G., Donny, A., Paul, B., Bruno, N., Jean-Louis, C., Olivier, P., Julien, O. and Bernard, V. (2015). *The flexible combined imager onboard MTG: from design to calibration.* Paper presented at the Proc.SPIE.